Memoirs of the Faculty of Engineering, Okayama University, Vol. 43, pp. 16-21, January 2009

FDTD Simulations of Acoustic Waves in Two-Dimensional Phononic Crystals using Parallel Computer

Tomoyuki KUROSE, Kenji TSURUTA *,
Chieko TOTSUJI, Hiroo TOTSUJI
Graduate School of Natural Science and Technology
Okayama University
Okayama 700-8530, Japan

(Received December 1, 2008)

The finite-difference time-domain (FDTD) method has been applied to the calculation of the phonon band structure of two-dimensional (2D) phononic crystals, consisting of metal cylinders placed periodically in liquid. By comparing several combinations of materials for metal cylinder and liquid, we analyze the dependence of the band structures on sound speed and density of liquid media. Moreover, the negative refraction of the acoustic waves is observed at the interfaces between phononic crystal slab and the liquid. We find that an acoustic " lens effect " with the slab appears due to the negative refractions. The relationship between the focal intensity in the lens effect and the band structure is discussed.

1 INTRODUCTION

In periodic, dielectric structures, so called photonic crystals, there are complete band gaps (photonic band gap) of electromagnetic waves. The analogy between photons and phonons has suggested a new class of materials, called phononic crystal or sonic crystal: It consits of periodic elastic composites of two or more materials [1]. It has attracted a great deal of interest in the study of the propagation of waves because of their novel physical properties.

Possible features of the photonic metamaterial, which has negative permittivity and permeability simultaneously, has been predicted in 1968 [2]. A negative refractive index is one of these features. Conventional optical lenses have positive refractive index, so it needs curved surfaces to get an image focused, whereas a negative refraction allows flat slab to focus electromagnetic waves [3]. Recently [4], this material, known also as a left-handed material, has been designed theoretically and experimentally [5]. The negative refraction behavior can also be achieved without negative permittivity/permeability or backward wave effect [6]. It is due to the negative photonic effective mass. In this case, the photonic crystal has an effective refractive index attributed to the photonic band structure. Such a photonic crystal behaves like a right-handed but unconventional medium.

Recently, analogous phenomena for acoustic and elastic wave propagation in phononic crystals have been predicted [1]. In Ref. [1], a negative refraction and an imaging effect of acoustic waves were achieved in the phononic crystal consisting of square arrays of rigid or liquid cylinders embedded in air background. Also, an acoustic negative refraction was observed experimentally in steel cylinders placed in air background [7,8]. Computer simulation [9] also supports that the phononic crystal, consisting of a hexagonal array of steel cylinders in air back ground, exhibits the acoustic lens effect. This effect is expected to lead to novel mechanisms for acoustic devices, acoustic sensors, and acoustic energy carriers to piezoelectric generator, for example.

In the present study, we calculate the dispersion relations of phonons and equivalent frequency surface (EFS) of 2D phononic crystals, which consist of metal cylinders embedded in liquid base, using the finite-difference time-domain (FDTD) method. We demonstrate existence of the negative refraction of acoustic waves at the interface of the liquid and the phononic crystal slab. Frequency range for the negative refrac-

*Email:tsuruta@elec.okayama-u.ac.jp

tion is shown to be controlled by the liquid base.

2 BASIC FORMALISM

2.1 Theory

We consider a 2D system consisting of infinitely long cylinders parallel to the z axis and the material parameters are independent on the coordinate z. The propagation of elastic wave are assumed to be only in $x-y$ plane. The elastic wave equation in such a system is written as

$$\rho\frac{\partial^2 u_x}{\partial t^2} = \frac{\partial \sigma_{xx}}{\partial x} + \frac{\partial \sigma_{xy}}{\partial y} \tag{1}$$

$$\rho\frac{\partial^2 u_y}{\partial t^2} = \frac{\partial \sigma_{xy}}{\partial x} + \frac{\partial \sigma_{yy}}{\partial y} \tag{2}$$

where u_x, u_y are the $x-$ or $y-$ component of the displacement and ρ is the mass density. The stress tensor $\sigma_{ij}(i,j=x,y)$ is represented as

$$\sigma_{xx} = C_{11}\frac{\partial u_x}{\partial x} + C_{12}\frac{\partial u_y}{\partial y} \tag{3}$$

$$\sigma_{xy} = C_{44}\left(\frac{\partial u_y}{\partial x} + \frac{\partial u_x}{\partial y}\right) \tag{4}$$

$$\sigma_{yy} = C_{11}\frac{\partial u_y}{\partial y} + C_{12}\frac{\partial u_x}{\partial x} \tag{5}$$

where C_{11}, C_{12} and C_{44} are elastic constants which depend on the position. In an isotropic system, these are related to the longitudinal and transverse speeds of wave c_l and c_t as $C_{11}=\rho c_l^2$, $C_{44}=\rho c_t^2$ and $C_{12}=C_{11}-2C_{44}$.

2.2 Band Calculation with FDTD Method

We then solve the elastic wave equation in real space and time with initial conditions using the FDTD algorithm [10]. The FDTD method is a powerful tool to deal with the wave transmission problem in finite size composites. The FDTD algorithm is based on discretization of the equation in spatial and time domain. In addition, the FDTD method is able to calculate the dispersion relations of phonons [11]. The calculation flow is shown in Fig.1. The Bloch theorem, owing to the periodicity, is

$$u(\mathbf{r},t) = e^{i\mathbf{k}\cdot\mathbf{r}}U(\mathbf{r},t) \tag{6}$$

$$\sigma(\mathbf{r},t) = e^{i\mathbf{k}\cdot\mathbf{r}}S(\mathbf{r},t) \tag{7}$$

where $\mathbf{r}=(x,y)$ is a position in $x-y$ plane, $\mathbf{k}=(k_x,k_y)$ is a Bloch wave vector, and $U(\mathbf{r},t)$ and $S(\mathbf{r},t)$ are periodic functions which satisfy $U(\mathbf{r}+\mathbf{a},t)=U(\mathbf{r},t)$ and $S(\mathbf{r}+\mathbf{a},t)=S(\mathbf{r},t)$ with $\mathbf{a}$ being a lattice translation vector. After the stationary state is reached, temporal spectra of the displacements are Fourier-transformed to frequency domain. We then identify the eigenfrequency at a given wave vector by finding the peaks in the frequency spectra as depicted in Fig. 2. Among many peaks in the frequency spectra, we only plot the first peaks in the band diagrams to be shown in the following sections. We perform the FDTD run for 2^{21} time steps for each wave vector.

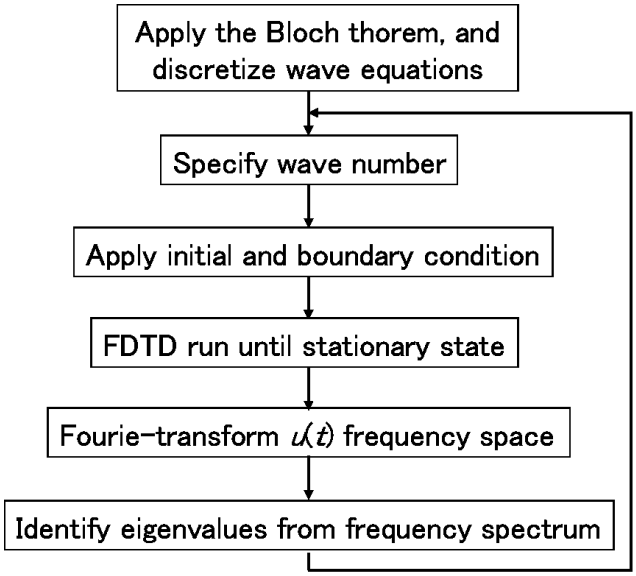

Fig. 1: Band calculation flow with FDTD method.

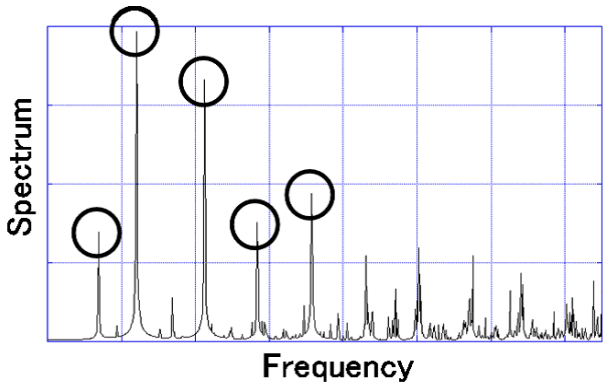

Fig. 2: Frequency spectra at a wave vector. Circles indicate the peaks corresponding to eigenfrequencies.

2.3 Boundary Condtion

The transmission properties are also investigated by the FDTD method. Sinusoidal incident waves are generated at a line source placed in liquid bases. Intensity of the transmitted waves is calculated by time-averaging of amplitude of the displacement. To calculate it, we apply the perfectly matched layer (PML) absorbing boundary condition [12]. In the PML region, the fields are split into x and y components, and Equation (1) is written as

$$\rho\left(\frac{\partial^2 u_x^x}{\partial t^2} + d^x\frac{\partial u_x^x}{\partial t}\right) = \frac{\partial \sigma_{xx}}{\partial x} \tag{8}$$

$$\rho\left(\frac{\partial^2 u_x^y}{\partial t^2}+d^y\frac{\partial u_x^y}{\partial t}\right)=\frac{\partial \sigma_{xy}}{\partial y} \tag{9}$$

and Equation (3) is written as

$$\frac{\partial \sigma_{xx}^x}{\partial t}+d^x\sigma_{xx}^x=C_{11}\frac{\partial^2 u_x}{\partial x\partial t} \tag{10}$$

$$\frac{\partial \sigma_{xx}^y}{\partial t}+d^y\sigma_{xx}^y=C_{12}\frac{\partial^2 u_y}{\partial y\partial t} \tag{11}$$

where d_x and d_y are attenuation factors. Other equations are similarly derived.

2.4 MPI Parallel Clculation

In this study, we use the message passing interface (MPI) for parallel calculations to simulate larger system efficiently. MPI is now a standard library for implementing parallel processing for various programming languages. Figure 3 shows the schematics of parallelization of FDTD grids. We decompose the space into subdomains and assign them to each central processing unit (CPU). In Fig. 3, for example, we separate the 2D space into four subdomains along y direction. In FDTD simulation, calculated data (such as u_x and u_y) at each boundary of rank are exchanged and updated at each time step.

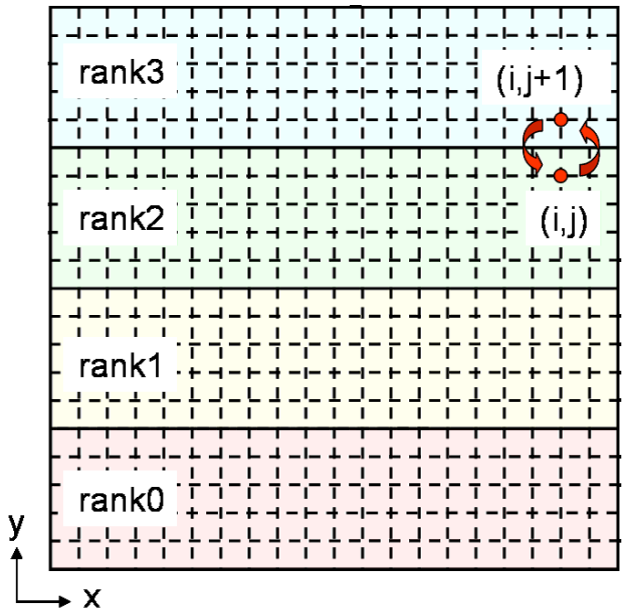

Fig. 3: Schematics of parallelization in FDTD simulation. 2D space is discretized to FDTD grids (dashed line) and decomposed into each rank (continuous line)

3 RESULTS

3.1 Band Structure

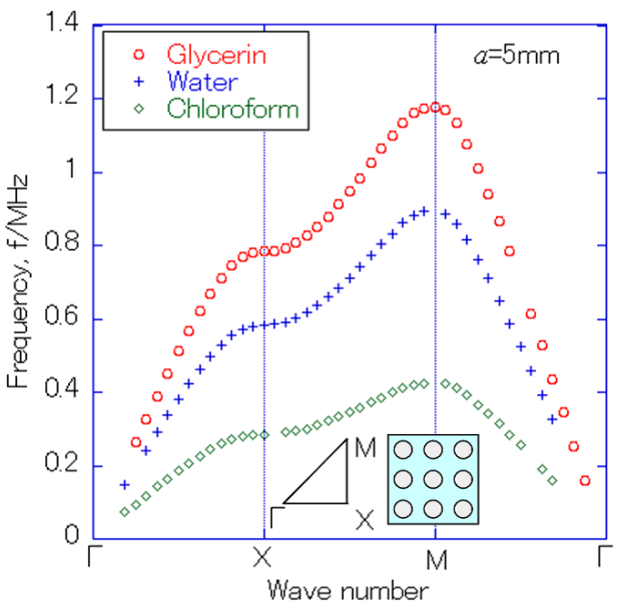

Fig. 4: First band structure for phononic crystals consisting of tungsten cylinders placed in glycerin, water, and chloroform, respectively. Inset shows a square lattice and its Brillouin zone.

In the present study, we first fix the material for the solid cylinders in the phononic crystals and change the liquid media to extract the dependence of the phononic properties on the relative density and sound speed. Tungsten is chosen as the material for the cylinders. The mass density and sound speeds of tungsten and liquids are as follows: ρ=19.3 g/cm^3, c_l=5.09 km/s, c_t=2.8 km/s for tungsten; ρ=1.0 g/cm^3, c_l=1.49 km/s for water; ρ=1.26 g/cm^3, c_l=1.98 km/s for glycerin; ρ=1.48 g/cm^3, c_l=0.995 km/s for chloroform, respectively. We select these liquids because these have roughly the same density, while the sound speeds are rather different. The filling fraction of cylinders is fixed at 50% and lattice constant is a=5mm.

Figure 4 shows the first phonon band of the systems with three different liquids. They all have a nearly symmetrical peak with respect to the wave vector at the M point in the first Brillouin zone. This feature is essential to cause the acoustic negative refraction. Moreover, the first band is low lying when the sound speed is small. This indicates that negative refraction frequency can be controlled by choice of the liquid media.

Figure 5 shows the EFS for the tungsten phononic crystal in the water. We find that a nearly circular EFS is formed around the M center of the first band. Such a circular EFS leads to the all-angle negative refractions and, in turn, to the refocusing of the transmitted waves, because at every k-point on this circle, the gradient $d\omega/d\mathbf{k}$ is pointing to the M center (see Sec. 3.2). We thus expect to observe the lens effect around the incident frequency f=0.65 MHz.

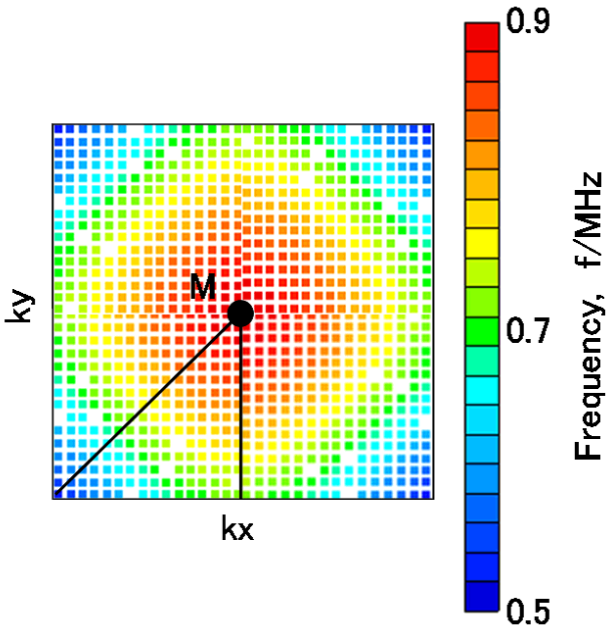

Fig. 5: EFS around M point in the band structure of phononic crystal consisting of tungsten cylinders placed in water.

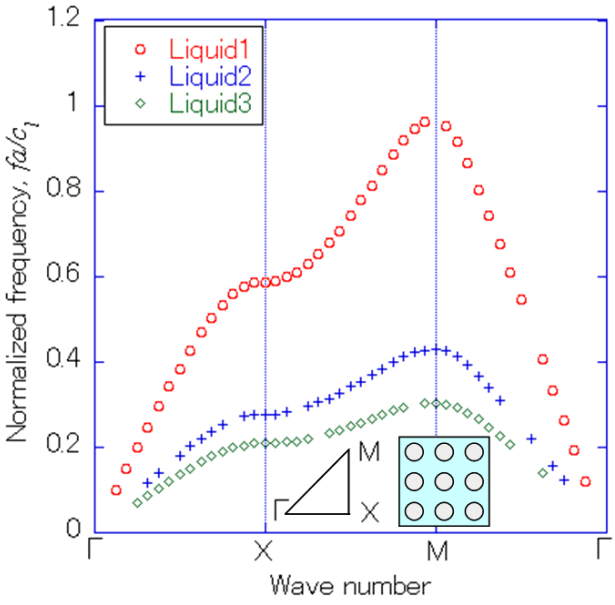

Fig. 6: First band structure of phononic crystals consisting of metal cylinders placed in different relative density; 0.01, 0.05, and 0.1. Inset shows a square lattice and its Brillouin zone. Frequency is normalized to fa/c_l, where c_l is the longitudinal sound speed of metal and a is the lattice constant.

Next, we investigate the dependence of the band structure on the relative density of the liquid media to the metal cylinder. In this case, we select the liquid materials with roughly the same sound speeds. The relative densities of the liquids are expressed as $\rho = \alpha\rho_0$, where ρ_0 is metal cylinder's density. We change the parameter as α=0.01, 0.05 and 0.1 for liquid1, liquid2 and liquid3, respectively. We fix the ratio of elastic constant C_{11} as metal:liquids = 1:10^{-3}. The filling fraction of cylinders is fixed at 50% same as in the previous section. We can see from Fig. 6 that as the relative density is smaller such as liquid1, the peak at the M point is higher than the others.

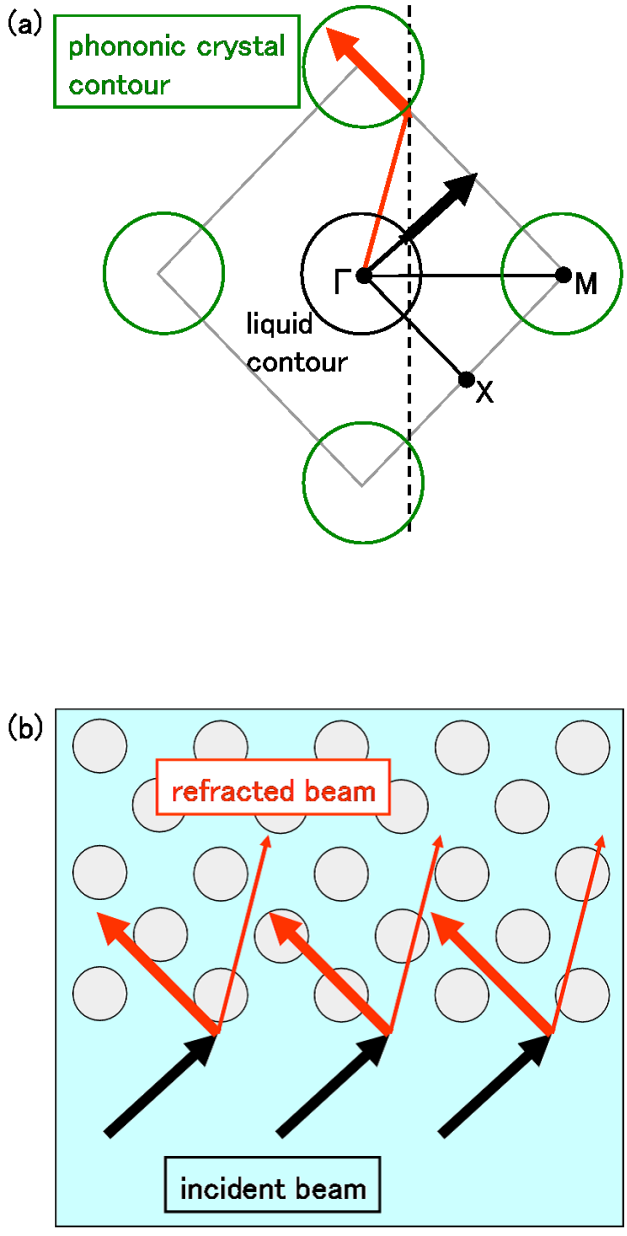

Fig. 7: (a): Negative refraction with equivalent frequency surface (EFS) and conservation of the wave vector parallel to the interface. Thick arrows indicate group velocity direction and thin arrows indicate phase velocity direction. (b): Diagram of refract direction in the real space.

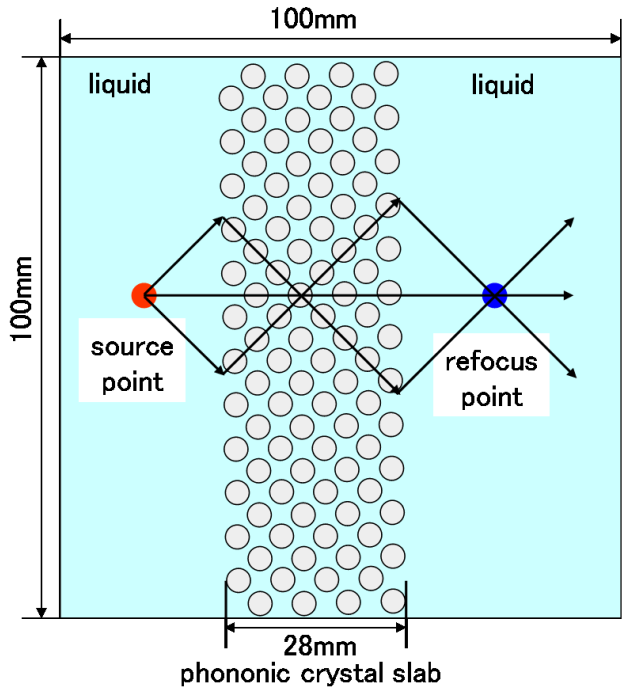

Fig. 8: Schematics of phononic crystal slab which has negative refractive index $n = -1$.

In this figure, the frequency f is normalized to fa/c_l, where c_l is the longitudinal sound speed of the metal and a is the lattice constant. It indicates that the negative refraction frequency can also be controlled by the relative density of liquid base.

3.2 Negative Refraction

Next, we demonstrate the negative refraction and the resulting acoustic lens effect by phononic crystal slab via FDTD simulations. Figure 7 illustrates schematically the wave propagation directions in reciprocal space and real space. When incident beam is emitted from liquid, the refracted mode is determined by the conservation of the wave vector parallel to the interface, and the refracted wave direction is determined by the circular EFS. If the slab is placed in a liquid with the surface normal to the ΓM direction and the contour is everywhere circular, an incoming wave from liquid propagating into the phononic crystal refracts to the negative side of the surface normal.

The simulation setup is shown in Fig. 8. Figure 8 also shows the schematics of the negative refraction and the lens effect. There are 8 layers of tungsten cylinders in the slab.

A line source is placed at the left side of the slab, and the phononic crystal slab is placed in a liquid with the surface normal to the ΓM direction. Acoustic waves are emitted from the line source and propagate into the 2D phononic crystal slab, which has negative refractive index $n = -1$. The transmitted waves are then refocused at the right side of the slab.

In Fig. 9, we can see that the acoustic waves are focused at the right side of the phononic crystal slab in the water. The incident acoustic wave frequency is at f=0.65 MHz, as we expect the negative refraction from band structure in Fig. 4.

Figure 10 shows the acoustic lens effect by the phononic crystal in liquid2. Normalized frequency of the incident wave is 0.32, at which we expect the negative refraction from the band-structure analysis. In contrast to Fig. 9, the focal intensity is rather weak due to the nonsymmetrical shape of the EFS around the M point in its band structure.

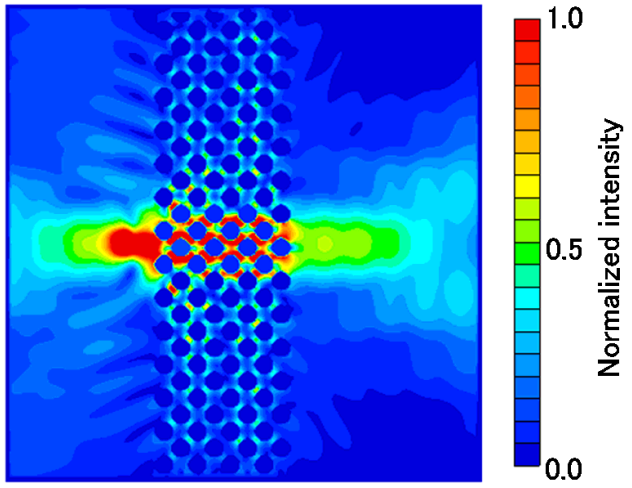

Fig. 9: Time average of normalized intensity distributions of displacement field. Eight layer tungsten cylinders are placed in water. Incident frequency is all the same at f=0.65MHz.

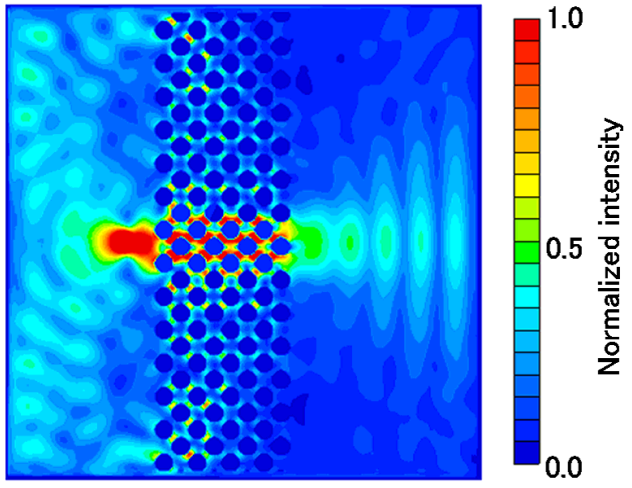

Fig. 10: Same as Fig. 8, but for metal cylinders placed in liquid2. Incident normalized frequency is 0.32.

4 SUMMARY

In summary, we investigated the dispersion relations

of the 2D phononic crystals consisting of metal cylinders embedded in liquid base using the FDTD method. The frequency peak at the M point is changed by relative sound speed and density of liquid, thus negative refraction frequency can be controlled by designing the phonon band structure. The negative refraction is occurred at 0.65MHz in the case of tungsten phononic crystal with lattice constant a=5mm embedded in water. On the other hand, when using chloroform instead of water, it occurrs at about 0.3MHz. The acoustic lens effect is demonstrated by simulating spherical waves transmitting through a phononic crystal slab. The focal intensity depends on the shape of the EFS in the phononic band structure. Further analyses of the dependence on structures, such as shape of the cylinders, dimensionality of the crystals, etc., are in progress.

ACKNOWLEDGEMENTS

This work was supported by Grant-in-Aid for Scientific Research on Priority Areas " Nano Materials Science for Atomic Scale Modification 474 "from MEXT of Japan.

APPENDIX

In this appendix, we show the discretized equations which reflect the Bloch theorem in Eqs. (6) and (7) into Eqs. (1)-(5).

$$\frac{\rho^{l,m}}{(\Delta t)^2}[U_x^{l,m;n+1} - 2U_x^{l,m;n} + U_x^{l,m;n-1}] = K_{x1}S_{xx}^{l+(1/2),m;n} + K_{x2}S_{xx}^{l-(1/2),m;n} + K_{y1}S_{xy}^{l,m+(1/2);n} + K_{y2}S_{xy}^{l,m-(1/2);n} \quad (12)$$

$$\frac{\rho^{l+(1/2),m+(1/2)}}{(\Delta t)^2}[U_y^{l+(1/2),m+(1/2);n+1} - 2U_y^{l+(1/2),m+(1/2);n} + U_y^{l+(1/2),m+(1/2);n-1}] = K_{x1}S_{yx}^{l+1,m+(1/2);n} + K_{x2}S_{yx}^{l,m+(1/2);n} + K_{y1}S_{yy}^{l+(1/2),m+1;n} + K_{y2}S_{yy}^{l+(1/2),m;n} \quad (13)$$

$$S_{xx}^{l+(1/2),m;n} = C_{11}^{l+(1/2),m}[K_{x1}U_x^{l+1,m;n} + K_{x2}U_x^{l,m;n}] + C_{12}^{l+(1/2),m}[K_{y1}U_y^{l+(1/2),m+(1/2);n} + K_{y2}U_y^{l+(1/2),m-(1/2);n}] \quad (14)$$

$$S_{yy}^{l+(1/2),m;n} = C_{12}^{l+(1/2),m}[K_{x1}U_x^{l+1,m;n} + K_{x2}U_x^{l,m;n}] + C_{11}^{l+(1/2),m}[K_{y1}U_y^{l+(1/2),m+(1/2);n} + K_{y2}U_y^{l+(1/2),m-(1/2);n}] \quad (15)$$

$$S_{xy}^{l,m+(1/2);n} = S_{yx}^{l,m+(1/2);n} = C_{44}^{l,m+(1/2)}[K_{x1}U_y^{l+(1/2),m+(1/2);n} + K_{x2}U_y^{l-(1/2),m+(1/2);n} + K_{y1}U_x^{l,m+1;n} + K_{y2}U_x^{l,m;n}] \quad (16)$$

where (l, m) defines a 2D grid point with grid spacing Δx and Δy, n defines the time step with interspace Δt, and $K_{x1} = (ik_x\Delta x+2)/2\Delta x$, $K_{x2} = (ik_x\Delta x-2)/2\Delta x$, $K_{y1} = (ik_y\Delta y+2)/2\Delta y$ and $K_{y2} = (ik_y\Delta y-2)/2\Delta y$. The initial conditions, the displacement fields at $t = 0$, are chosen as

$$U_x^{l,m;0} = \delta_{l,l_0}\delta_{m,m_0} \quad (17)$$

$$U_y^{l+(1/2),m+(1/2);0} = 0 \quad (18)$$

where the grid point (l_0, m_0) is a random point in the unit cell.

REFERENCES

[1] X. D. Zhang and Z. Liu, Appl. Phys. Lett. **85** (2004) 341-343.
[2] V. G. Veselago, Sov. Phys. Usp. **10** (1968) 509-514.
[3] J. B. Pendry, Phys. Rev. Lett. **85** (2000) 3966-3969.
[4] P. Markos and C. M. Soukoulis, Phys. Rev. E. **65** (2002) 036622-036629.
[5] D. R. Smith, W. J. Padilla, D. C. Vier, S. C. Nemat-Nasser, and S. Schultz, Phys. Rev. Lett. **84** (2000) 4184-4187.
[6] C. Luo, S. G. Johnson, J. D. Joannopoulos, and J. B. Pendry, Phys. Rev. B **65** (2002) 201104-201107.
[7] L. Feng, X. -P. Liu, Y. -B. Chen, Z. -P. Huang, Y. -W. Mao, Y. -F. Chen, J. Zi, and Y. -Y. Zhu, Phys. Rev. B **72** (2005) 033108-033111.
[8] L. Feng X. -P. Liu, M. -H. Liu, Y. -B. Chen, Y. -F. Chen, Y. -W. Mao, J. Zi, Y. -Y. Zhu, S. -N. Zhu, and N. -B. Ming, Phys. Rev. B **73** (2006) 193101-193104.
[9] C. Qiu, X. Zhang, and Z. Liu, Phys. Rev. B **71** (2005) 054302-054307.
[10] A. Taflove and S. C. Hangess: *Computational Electrodynamics, The Finite-Difference Time-Domain Method, Third Edition*, (Artech House, London, 2005).
[11] Y. Tanaka, Y. Tomoyasu, and S. Tamura, Phys. Rev. B **62** (2000) 7387-7392.
[12] F. Chagla, C. Cabani, and P. M. Smith, Proc.-IEEE Ultrasonics Symposium **2004**, (2004) 517-520.